Developmental Biology 421 (2017) 258–270

Contents lists available at ScienceDirect

Developmental Biology

journal homepage: www.elsevier.com/locate/developmentalbiology

KirrelL, a member of the Ig-domain superfamily of adhesion proteins, is essential for fusion of primary mesenchyme cells in the sea urchin embryo

Charles A. Ettensohn*, Debleena Dey

Department of Biological Sciences, Carnegie Mellon University, 4400 Fifth Avenue, Pittsburgh, PA 15213, United States

ARTICLE INFO

Keywords:
Sea urchin embryo
Cell fusion
Primary mesenchyme cells
Skeleton
Morphogenesis
Gene regulatory network

ABSTRACT

In the sea urchin embryo, primary mesenchyme cells (PMCs) adhere to one another and fuse via filopodia, forming cable-like structures within which skeletal rods are deposited. Although this process was first described more than a century ago, molecules that participate in PMC adhesion and fusion have not been identified. Here we show that KirrelL, a PMC-specific, Ig domain-containing transmembrane protein, is essential for PMC fusion, probably by mediating filopodial adhesions that are a pre-requisite for subsequent membrane fusion. We show that KirrelL is not required for PMC specification, migration, or for direct filopodial contacts between PMCs. In the absence of KirrelL, however, filopodial contacts do not result in fusion. *kirrelL* is a member of a family of closely related, intronless genes that likely arose through an echinoid-specific gene expansion, possibly via retrotransposition. Our findings are significant in that they establish a direct linkage between the transcriptional network deployed in the PMC lineage and an effector molecule required for a critically important PMC morphogenetic process. In addition, our results point to a conserved role for Ig domain-containing adhesion proteins in facilitating cell fusion in both muscle and non-muscle cell lineages during animal development.

1. Introduction

The primary mesenchyme cells (PMCs) of the sea urchin embryo are a valuable experimental model for the analysis of cell fate specification, morphogenesis, and the evolution of development (Ettensohn, 2013; Lyons et al., 2014). PMCs undergo a spectacular sequence of well-described cell behaviors that culminates in the assembly of the skeletal system. Recently, important features of a gene regulatory network deployed in the PMC lineage have been elucidated (Oliveri et al., 2008; Rafiq et al., 2012, 2014; Barsi et al., 2014). It is therefore now feasible to identify direct connections between this gene regulatory program and the suite of morphogenetic processes that underlies skeletal development (Ettensohn, 2013; Rafiq et al., 2014; Saunders and McClay, 2014). Linking gene regulatory networks to morphogenetic processes will be essential for understanding the transformation of genotype into phenotype and for elucidating the evolution of developmental anatomy. The diversity of programs of skeletal development within the Echinoderm phylum affords an outstanding opportunity to address these issues (Erkenbrack and Davidson, 2015; Koga et al., 2016).

PMC fusion was first described more than a century ago (Théel, 1892). Subsequently, light and electron microscopic observations showed that the formation of the PMC syncytium involves the fusion and progressive amalgamation of protrusions (filopodia and thicker cell processes known as pseudopodia) extended by these cells (Gustafson and Wolpert, 1961; Okazaki, 1965; Gibbins et al., 1969). This mode of fusion produces a syncytium that consists of roughly spherical PMC bodies attached by slender stalks to a membrane-bounded, cable-like strand of cytoplasm (the latter is referred to herein as the "pseudopodial cable"). Hodor and Ettensohn (1998) used time-lapse confocal imaging and dye transfer assays to analyze the dynamics of PMC fusion in *Lytechinus variegatus*. They found that fusion is initiated soon after PMCs begin to migrate and that all PMCs are joined in a common syncytium by the mid-gastrula stage. They also showed that PMC fusion involves cell type-specific recognition mechanisms that are autonomously programmed in the founder cells of the PMC lineage very early in development. Together, these studies have led to a detailed picture of PMC fusion at the cellular level, but molecules that participate in PMC fusion have not been identified.

In the present study, we show that KirrelL, a PMC-specific member of the Ig-domain superfamily of cell adhesion proteins, is essential for PMC fusion. Our findings suggest that KirrelL functions in an early, cell recognition/adhesion step that is a pre-requisite for subsequent membrane fusion. Direct PMC-PMC filopodial contacts occur in

* Corresponding author.
E-mail address: ettensohn@cmu.edu (C.A. Ettensohn).

http://dx.doi.org/10.1016/j.ydbio.2016.11.006
Received 8 October 2016; Received in revised form 1 November 2016; Accepted 1 November 2016
Available online 17 November 2016
0012-1606/

KirreL morphants, but such contacts do not result in membrane fusion. *KirrelL* is a member of a family of closely related genes that likely arose through an echinoid-specific gene expansion, possibly via retrotransposition. Knockdowns of the four PMC-specific members of this family show that only KirrelL is essential for cell fusion, although a different protein in the family (IgTM) plays an important role in skeletal morphogenesis by regulating the number of initial branches that arise within each skeletal primordium. Our findings are important in that they establish a direct linkage between the transcriptional network deployed in the PMC lineage and an effector gene required for cell-cell fusion, one of the key morphogenetic processes that underlies skeletal development. In addition, our results point to a conserved role for Ig domain-containing adhesion proteins in facilitating cell fusion in both muscle and non-muscle cell lineages during animal development.

2. Materials and methods

2.1. Embryo culture

Adult *Lytechinus variegatus* were obtained from the Duke University Marine Laboratory (Beaufort, NC, USA) or Reeftopia, Inc. (Key West, FL, USA). Adult *Strongylocentrotus purpuratus* were obtained from Pat Leahy (California Institute of Technology, Pasadena, CA, USA). Spawning was induced by intracoelomic injection of 0.5 M KCl and embryos were cultured in artificial seawater (ASW) at 23 °C (*L. variegatus*) or 15 °C (*S. purpuratus*).

2.2. Morpholino (MO) and mRNA injections

Translation-blocking MOs (Gene Tools, LLC, Philomath, OR) and mRNAs were injected into fertilized eggs as previously described (Cheers and Ettensohn, 2004). A C-terminal, GFP-tagged form of LvKirrelL was produced by cloning the full coding sequence into the BamHI and ClaI sites of the pCS2(+)GFP vector. Capped mRNA was synthesized using the SP6 mMessage mMachine RNA Transcription Kit (Life Technologies).

MO sequences were:

Lv-KirrelL: 5′-GGTTCATTCTTGCTGGACTGAATTT-3′
Sp-KirrelL: 5′-TATGGTTCATGCTGGCTTGAATGTC-3′
Lv-IgTM: 5′-TCCAGCATGATACCAAGACCCTCAT-3′
Sp-IgTM: 5′-ACCAATATCATCATGCTTCAAGGTC-3′
Lv-Hypp_1164: 5′-TGAACAGTAAAATAGTCCGCTCCAT-3′
Lv-Kirrel2l: 5′-ACCAAAGATTCCAGCAGGATGCCAT-3′

2.3. Immunofluorescence and whole mount in situ hybridization (WMISH)

Immunofluorescent staining using mAb 6a9 (a PMC-specific marker) and WMISH were carried out as previously described (Adomako-Ankomah and Ettensohn, 2013).

2.4. Cell fusion assays

PMC cell fusion was assayed as previously described (Hodor and Ettensohn, 2008). Briefly, to assess the organization of the PMC syncytium at the late gastrula stage, paraformaldehyde-fixed embryos were labeled with DiI and the embryos were stored overnight to allow the dye to diffuse throughout the syncytium. Cell fusion was also monitored directly in living embryos by intercellular transfer of fluorescent dextran. In these studies, small numbers of PMCs were transplanted from dextran-labeled donor embryos into unlabeled host embryos and fusion was assayed by transfer of the cytoplasmic dye from donor to host PMCs.

2.5. Quantification of filopodial numbers and lengths

PMCs were isolated microsurgically from *L. variegatus* embryos and cultured on fibronectin-coated coverslips as described by Adomako-Ankomah and Ettensohn (2013). Cells were allowed to attach for 1 h in plain seawater and high-resolution images of randomly selected fields of cells were then collected using a differential interference contrast (DIC) 40X oil lens (N.A.=1.3) and an Olympus DP71 digital camera. Measurements of filopodial lengths were made using the segmented line measurement tool of ImageJ. For filopodia that did not have a visible pseudopodial root, measurements were made from the edge of the cell body to the tip of the filopodium. For filopodia that extended from a broad pseudopodial base, measurements were made from the approximate center of the pseudopodium to the filopodial tip.

2.6. Phylogenetic tree construction

Maximum likelihood (ML) trees were constructed using Guidance (http://guidance.tau.ac.il) (Penn et al., 2010) and MEGA5 (v. 5.2.2) (Tamura et al., 2011; Hall, 2013), as described by Ettensohn (2014). The ML method is widely used for tree construction (De Bruyn et al., 2014) and we chose to generate unrooted trees because it was difficult to identify a protein sequence that could serve as an appropriate outgroup. Briefly, Guidance was used to generate MAFFT-based multiple sequence alignments (MSAs) and amino acids that could not be aligned with confidence (columns with Guidance scores < 0.25) were removed. MEGA5 was used to determine the optimal substitution model and to construct maximum likelihood (ML) trees without any further deletion of gaps and with a bootstrap value of 500. All proteins sequences used for tree construction are contained in Supplemental File 1.

3. Results

3.1. Identification of PMC-specific, Ig-domain transmembrane proteins

In a previous study (Rafiq et al., 2014) we used RNAseq to identify targets of Sp-Alx1 and Sp-Ets1, two transcription factors that play pivotal roles in PMC specification. Manual curation of genes that were positively regulated by both Alx1 and Ets1 led to the identification of three mRNAs that encoded Type I transmembrane proteins with multiple extracellular Ig domains. Two of these mRNAs, *Sp-kirrelL* (SPU_024995) and *Sp-hypp_1164* (SPU_026000) had been previously annotated, while the third represented a previously unannotated gene (we originally designated this gene "*Sp-Scaffold17:88148-92454*" based on its coordinates in the *S. purpuratus* v3.1 genome assembly, but for simplicity this gene is referred to herein as "*Sp-IgTM*." All three mRNAs are expressed selectively by PMCs (Rafiq et. al., 2014). In the present study, further curation of the set of 420 PMC-enriched mRNAs using the SMART protein domain database (http://smart.embl-heidelberg.de/) revealed an additional gene (*Sp-kirrel2L*), not identified in the previous analysis, that also encodes a PMC-enriched, Ig domain-containing transmembrane protein. Like the other three genes, *Sp-kirrel2L* is regulated positively by Alx1 and Ets1.

The domain organization of the four proteins is illustrated in Fig. 1. Each contains a predicted signal sequence, 2–3 extracellular Ig domains, a single transmembrane domain, and a cytoplasmic region that lacks identifiable domains. The corresponding genes, *Sp-IgTM*, *Sp-kirre1L*, *Sp-hypp_1164*, and *Sp-kirre2L*, are located on four separate genomic scaffolds and are flanked by unrelated genes. All four genes lack introns. Based on RNAseq data (Rafiq et al., 2014), the order of abundance of the four PMC-enriched mRNAs at the early gastrula stage is: *Sp-IgTM* > *Sp-kirrelL* > *Sp-hypp_1164* > *Sp-kirre2L*, with expression levels that correspond to approximately 15, 6, 2, and 1

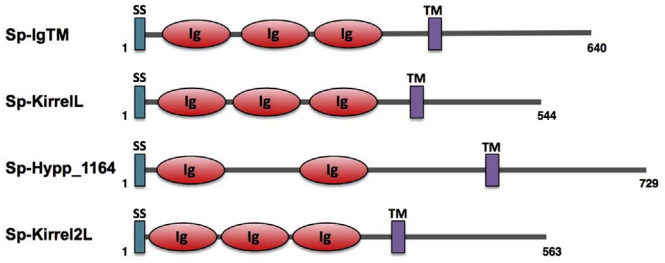

Fig. 1. Domain organization of Sp-IgTM, Sp-KirrelL, Sp-Hypp_1164, and Sp-Kirrel2L. Signal sequences were identified using SignalP 4.1 (www.cbs.dtu.dk/services/SignalP) and additional domains were annotated using SMART (http://smart.embl-heidelberg.de/), CDD (http://www.ncbi.nlm.nih.gov/cdd/), and Pfam (http://pfam.xfam.org/), with default parameters. The subclassification of Ig domains (e.g., as Ig, Ig-like, or Igc2 domains) varied among domain annotation tools and is therefore not shown. Ig=immunoglobulin domain, SS=signal sequence, TM=transmembrane domain.

molecules/PMC, respectively (assuming 32 PMCs/embryo). Two of these genes (*Sp-kirrelL* and *Sp-kirrel2L*) were included in the developmental time course analysis of Tu et al. (2014). Both mRNAs begin to accumulate at ~18 h of development, peak at the early gastrula stage (~30 h), and then decline in expression, a temporal pattern characteristic of many genes that are expressed selectively by PMCs and co-regulated by Alx1 and Ets1 (Rafiq et al., 2014).

3.2. KirrelL is required for the formation of the PMC pseudopodial cable

We previously developed cell fusion assays that allowed us to study the dynamics of PMC fusion in *Lytechinus variegatus* embryos (Hodor and Ettensohn, 1998, 2008), which are more amenable to microsurgical manipulations and light optical imaging than embryos of *S. purpuratus*. To employ these assays, we first identified orthologs of IgTM, KirrelL, Hypp_1164, and Kirrel2L in *L. variegatus* by searching a public collection of transcripts and genomic scaffolds (www.echinobase.org) (Cameron et al., 2009). Each pair of orthologous proteins exhibited a high degree of sequence conservation (Fig. 10, Supp. Fig. 1) and all four *Lytechinus* genes lack introns. We analyzed the expression of *IgTM* and *kirrelL* (the two most abundant of the four mRNAs in *S. purpuratus*) in *L. variegatus* embryos by WMISH and confirmed that these genes are expressed selectively by PMCs during gastrulation (Supp. Fig. 2).

Knockdown of Lv-KirrelL had a striking and highly reproducible effect on skeletal morphogenesis (Fig. 2). Embryos injected with 1 mM LvKirrelL MO (which corresponded to a concentration in the egg cytoplasm of 1–2 μM) hatched and initiated gastrulation at the same time as uninjected, sibling embryos. PMCs migrated away from the vegetal plate on schedule and, by the late gastrula stage, became arranged in a circumferential pattern that consisted of two ventrolateral clusters (VLCs) joined by ventral and dorsal bands of PMCs (Fig. 2I, I′). Although the PMCs adopted a ring-like pattern in Lv-KirrelL morphants, the cells did not become aligned in chains but instead were more dispersed (Fig. 2J-J′). At post-gastrula stages of development, when control embryos formed extensive, branched skeletons, Lv-KirrelL morphants lacked skeletal elements or formed short linear or branched rods that were scattered throughout the bands of loosely associated PMCs (Fig. 2G′, J′). After 4 days of development, when sibling controls reached the late pluteus stage, Lv-KirrelL morphants exhibited a normal morphology except for their reduced skeletons; i.e., they developed coelomic pouches, a compartmentalized gut, a mouth, a well-formed ciliary band, and dorsal pigmentation.

During normal development, PMC fusion is accompanied by the formation of a pseudopodial cable that forms from the coalescence of filopodial and pseudopodial protrusions (Gustafson and Wolpert, 1961; Okazaki, 1965; Gibbins et al., 1969). The PMC pseudopodial cable was readily apparent in control late gastrula or prism stage embryos but was strikingly absent from LvKirrelL morphants. Immunostaining of fixed whole mounts with monoclonal antibody (mAb) 6a9, which specifically labels PMC membranes, confirmed that PMCs migrated to appropriate target sites in morphant embryos but adopted a loose configuration and failed to form a pseudopodial cable (Fig. 3).

The penetrance and dose-dependence of the KirrelL morphant phenotype was examined in two independent trials. Morphant embryos were examined by DIC and polarization microscopy when control embryos reached the prism stage. At injection concentrations of 2 mM, 1 mM, or 500 μM, 70–80% of injected embryos lacked any visible skeletal elements or formed only small, birefringent granules. All remaining morphant embryos (20–30%) exhibited one or more skeletal rods, but these were always short. At a MO concentration of 250 μM, most embryos formed multiple, small skeletal rods, while some (20%) formed two normal, branched spicules. At the lowest concentration tested (125 μM), most embryos (82%) formed normal skeletal elements. Based on these findings, MO concentrations of 1 or 2 mM were used for all subsequent experiments.

Knockdown of KirrelL in a different sea urchin species, *S. purpuratus*, produced an identical phenotype (Fig. 4). PMCs adopted a loose ring pattern but did not associate tightly with one another, failed to form a pseudopodial cable, and deposited small, scattered skeletal elements. The Sp-KirrelL MO exhibited a dose dependent effect very similar to that of the Lv-KirrelL MO, and the morphant phenotype was highly penetrant at injection concentrations of 1–2 mM. These findings revealed a conservation of KirrelL function in *S. purpuratus* and *L. variegatus*, two sea urchin species separated by ~100 million years (MY) (Smith et al., 2006). Moreover, because the two TB-MOs differed significantly in sequence (9/25 residues), and because MO binding is highly sensitive to mismatches (Summerton, 1999), these experiments indicated that the characteristic morphant phenotype was due a specific inhibition of KirrelL function rather than an off-target effect.

3.3. KirrelL is essential for PMC fusion

The loose arrangement of PMCs within the subequatorial ring pattern and the absence of a pseudopodial cable indicated that the cells were not joined in a syncytial network. To confirm that this was the case, morphant and control *L. variegatus* embryos were fixed with paraformaldehyde at the late gastrula stage and a DiI-coated needle was pressed against one VLC, labeling a small number of PMCs (Hodor and Ettensohn, 1998; Fig. 5). The fixed embryos were then stored overnight at 4 °C to allow the DiI to diffuse. In control embryos, DiI diffused throughout the PMC ring (16/16 cases). In contrast, in embryos injected with 2 mM Lv-Kirrell MO, the dye always remained restricted to the VLC that was originally labeled (28/28 cases). Multiple cells (6–8 cells, on average) were labeled in these VLCs after overnight incubation, but other PMCs in the same cluster remained unlabeled. Presumably most or all of the cells that were fluorescent after overnight incubation had been labeled by the DiI-coated needle at the start of the procedure, although it is possible that a limited transfer of dye to a few cells occurred. In any case, the results of DiI labeling studies showed clearly that in Lv-KirrelL morphants, PMCs were not organized in a syncytial network at the late gastrula stage.

The absence of a PMC syncytium in KirrelL morphants strongly suggested that PMC fusion was blocked. It remained formally possible, however, that transient membrane fusion events occurred earlier in development but were unstable, thus preventing the formation of a persistent syncytial network. This possibility could not be excluded *a priori*, as PMC fusion is sometimes reversible, at least *in vitro* (Karp and Solursh, 1985a). To test directly whether KirrelL was required for PMC fusion, fluorescein dextran-labeled PMCs were transplanted into unlabeled hosts and cell fusion was monitored in living embryos by intercellular dye transfer (Hodor and Ettensohn, 1998; Fig. 6). As reported previously, when 2–5 fluorescent dextran-labeled PMCs were

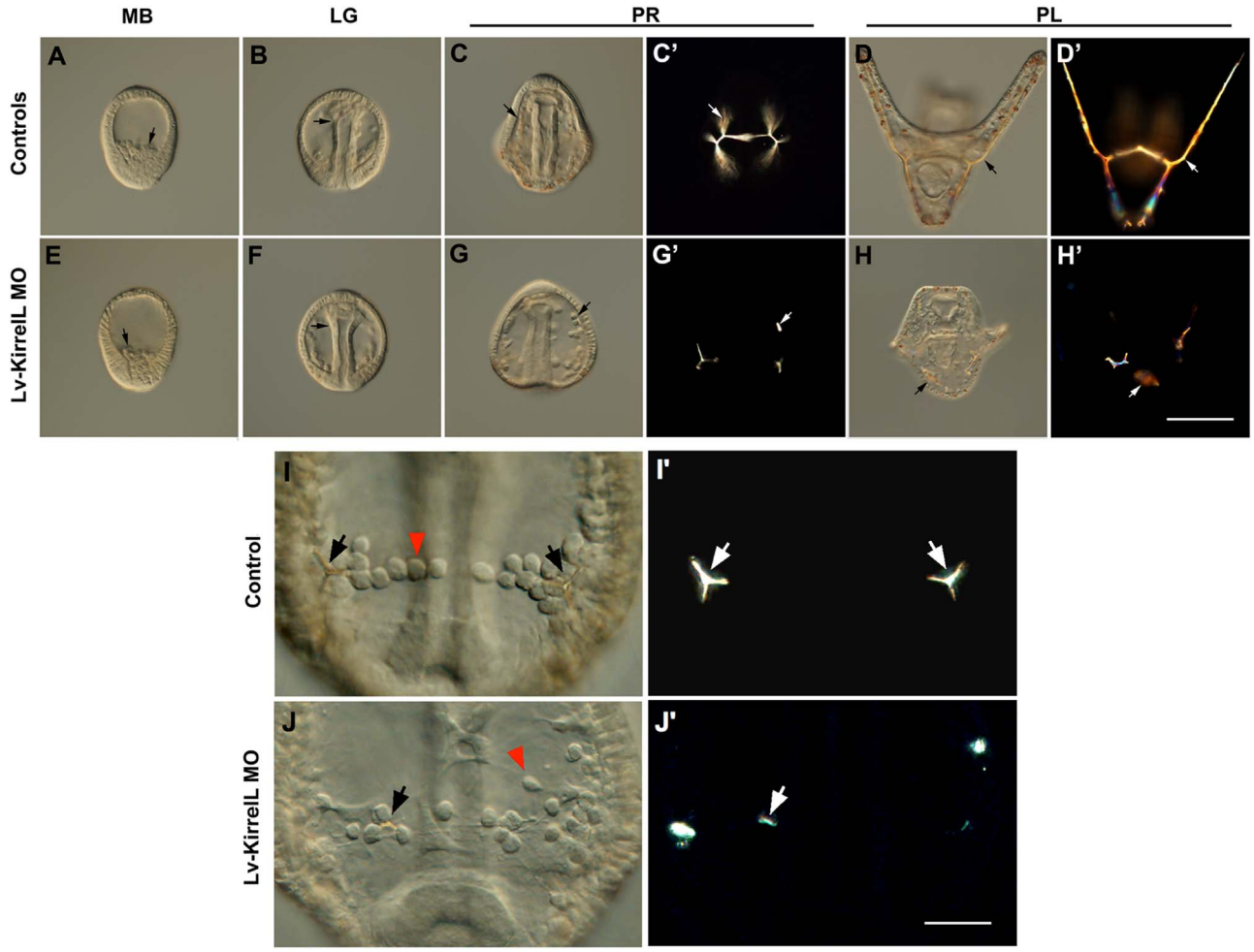

Fig. 2. Effects of Lv-KirrelL knockdown on PMC patterning and skeletogenesis. All images are of living embryos. At late embryonic stages, paired DIC and polarized light images of the same embryo are shown (e.g., C and C′). Upper panels show control, uninjected embryos (A–D′) and sibling Lv-KirrelL morphants (1 mM) (E–H′) at the mesenchyme blastula (MB), late gastrula (LG), prism (PR) and pluteus (PL) stages. PMCs ingressed on schedule in Lv-KirrelL morphants (arrows, A, E) and the archenteron invaginated normally (arrows, B, F). PMCs migrated away from the vegetal plate in both control and morphant embryos. They gave rise to an extensive, branched skeleton in control embryos (arrows, C, C′, D, and D′) but deposited only scattered, small, birefringent skeletal elements in Lv-KirrelL morphants (arrows, G, G′, H, and H′). Lower panels (I-J′) show high magnification, ventral views of a control (uninjected) and sibling Lv-KirrelL morphant embryo (1 mM) at the late gastrula stage. In control embryos, the PMCs were organized in tight cellular chains (red arrowhead, I) and in compact VLCs within which tri-radiate skeletal rudiments were deposited (arrows, I, I′). In contrast, in LvKirrelL morphant embryos, PMCs were arranged in a circumferential pattern at the correct position along the blastocoel wall, but the cells appeared very loosely associated with one another (red arrowhead, J). They were not aligned in tight cellular chains nor did they form compact VLCs. Small skeletal elements (arrows, J, J′) were apparent at various locations within the loosely organized PMC pattern. Scale bars=100 μm (A–H′) and 25 μm (I–J′).

transplanted from a control embryo into an unlabeled, control host, within 12 h the dextran spread throughout the entire PMC syncytium (10/10 cases). In contrast, transplantation of 2–5 dextran-labeled PMCs from a Lv-KirrelL morphant into an unlabeled, morphant host resulted in little or no dye transfer. Most embryos (16/26, or 62%) still had 2–5 labeled PMCs after 12 h. 38% of the embryos (10/26) had 6–15 labeled cells and in no case were more than 15 cells labeled (note that there are ~64 PMCs/embryo in *L. variegatus* at the late prism stage, when the embryos were scored). A similar inhibition of cell fusion was observed when PMCs were transplanted from morphant donors into control hosts: 16/23 embryos (70%) had 1–5 labeled cells, and 7/23 (30%) had 6–15 labeled cells after 12 h. These findings showed that 1) KirrelL is essential for PMC fusion, and 2) KirrelL is required in both fusion partners.

3.4. KirrelL is required for filopodial contacts to result in membrane fusion

The effect of KirrelL knockdown on PMC fusion might be a consequence of disrupting the formation or motility of filopodia, which mediate PMC fusion (Gustafson and Wolpert, 1961; Okazaki, 1965; Hodor and Ettensohn, 1998). Our initial observations suggested this was unlikely because in morphant embryos, PMCs migrated away from the vegetal plate and adopted a ring-like configuration, demonstrating that the cells were motile and responsive to guidance cues such as VEGF (Duloquin et al., 2007; Adomakoh-Ankomah et al., 2013). To visualize PMC filopodia directly, living and immunostained Lv-KirrelL morphant embryos were examined by DIC and fluorescence microscopy, respectively (Fig. 7A–D). We observed that PMCs in Lv-KirrelL morphants had a typical migratory morphology, with numerous filopodia that projected from broader protrusions (pseudopodia) proximal to the cell body. A meshwork of slender filopodia was visible within the loosely organized strands of PMCs that formed in these embryos, although a pseudopodial cable did not form (Fig. 7C). Direct interactions between the filopodia of neighboring PMCs were frequently observed (Fig. 7B, D). These observations strongly suggested that the inability of PMCs to form a syncytium was not due to a defect in the formation or motility of PMC filopodia.

To quantify features of filopodial behavior, we examined isolated, living PMCs cultured on fibronectin-coated coverslips (Fig. 7E, F). This provided a two-dimensional environment for the cells and allowed accurate measurements of filopodial numbers and lengths. It was

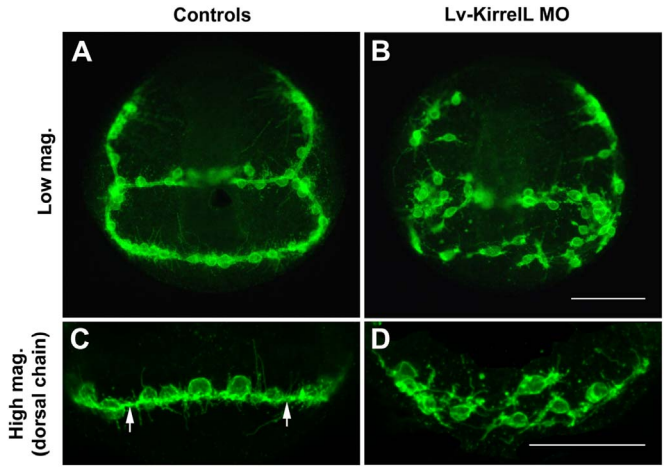

Fig. 3. Absence of PMC chains and pseudopodial cables in LvKirrelL morphants. 6a9-immunostained whole mounts showing the arrangement of PMCs in control prism stage embryos (A, C) and sibling Lv-KirrelL morphant embryos (2 mM) (B, D). Low and high magnification views show different embryos. In control embryos, PMCs were aligned in chains and their cell bodies were connected to a distinct pseudopodial cable (arrows, C). In Lv-KirrelL morphants, a circumferential band of PMCs, consisting of two VLCs joined by ventral and dorsal bands, was also apparent, but the PMCs were loosely arranged within the bands and a pseudopodial cable did not form. Scale bars =50 μm.

shown previously that PMCs extend numerous filopodia and migrate actively under these conditions (Karp and Solursh, 1985b; Adomako-Ankomah and Ettensohn, 2013). By mixing unlabeled and dextran-labeled cells, we found that normal PMCs fused actively in culture, with the earliest fusion events detectable < 1 h after plating, while PMCs isolated from KirrelL morphant embryos failed to fuse even after 4 h (Supp. Fig. 3). Both control and morphant PMCs attached to the substrate and extended numerous filopodia. The average number of filopodia per cell was not significantly different in control and morphant PMCs (4.2 and 4.5 filopodia/cell, respectively) (see Fig. 9; Table 1). Although we did not observe cells continuously, these data suggested that KirrelL knockdown did not affect the rate at which filopodia form. In addition, we detected only a small difference in the length of filopodia- on average, filopodia extended by morphant PMCs were ~14% shorter than filopodia extended by control PMCs. Together, our *in vivo* and *in vitro* data provide strong evidence that the inhibition of cell fusion in KirrelL morphants is not due to a failure of PMCs to extend filopodia or to contact neighboring cells. Instead, the fusion defect results from a failure of PMC filopodial contacts to support cell-cell fusion.

KirrelL is a Type I transmembrane protein and we hypothesized that it might be expressed on the PMC surface, where it could act as a cell recognition/adhesion molecule. Thus far, efforts to raise an anti-KirrelL antibody useful for immunolocalization studies have been unsuccessful. Therefore, as an alternative strategy, we expressed a GFP-tagged form of Lv-KirrelL in living cells (Fig. 8). In the epithelial cells of blastulae, the protein was highly concentrated at the cell periphery (Fig. 10, A–B′). When compared with membrane-bound GFP, the distribution of KirrelL-GFP was less tightly restricted to the plasma membrane; this was not unexpected, as mGFP is targeted directly to the plasma membrane via post-translational lipid modifica-

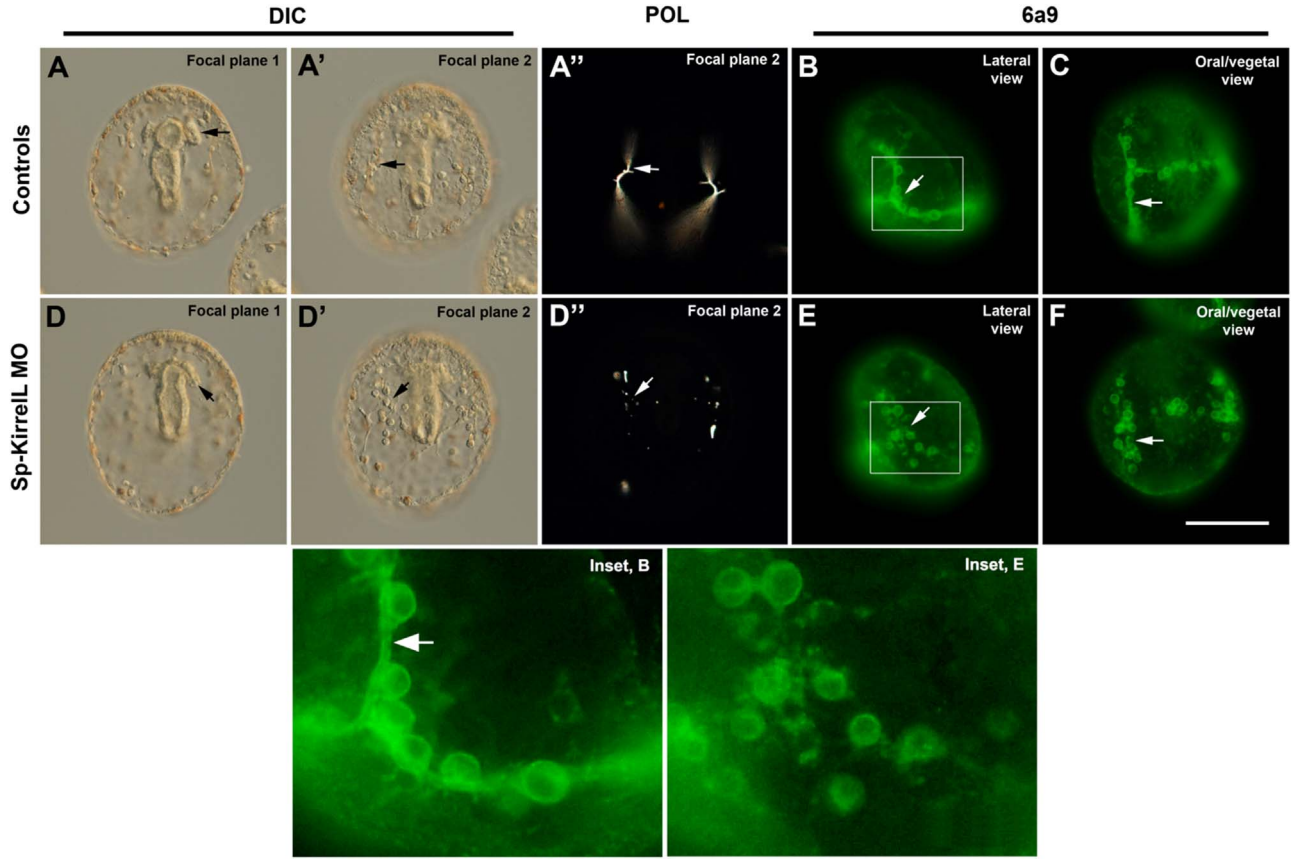

Fig. 4. Knockdown of KirrelL in *S. purpuratus*. Top panels (A–C)- Control (uninjected) embryos at the late prism stage. Bottom panels (D-F)- sibling morphant embryos (2 mM). A–A" and D–D" each show a single embryo viewed with DIC and polarized light (POL) microscopy. (B, C, E, F) – Four different embryos immunostained with mAb 6a9. Arrows in A and D indicate coelomic pouches; arrows in all other panels point to PMCs and/or skeletal elements. The phenotype of Sp-KirrelL morphants was indistinguishable from that of Lv-KirreL morphants. PMCs in control embryos were tightly organized in cellular chains and produced an extensive, branched skeleton (A'–C). By contrast, PMCs in Sp-KirrelL morphants were loosely associated with one another (D′, E, F), did not form a pseudopodial cable, and deposited only small, scattered birefringent elements (D"). Bottom panels show enlargements of the boxed regions in B and E. Arrow indicates the pseudopodial cable in the control embryo, which is lacking in the morphant. Scale bar=100 μm (A–F).

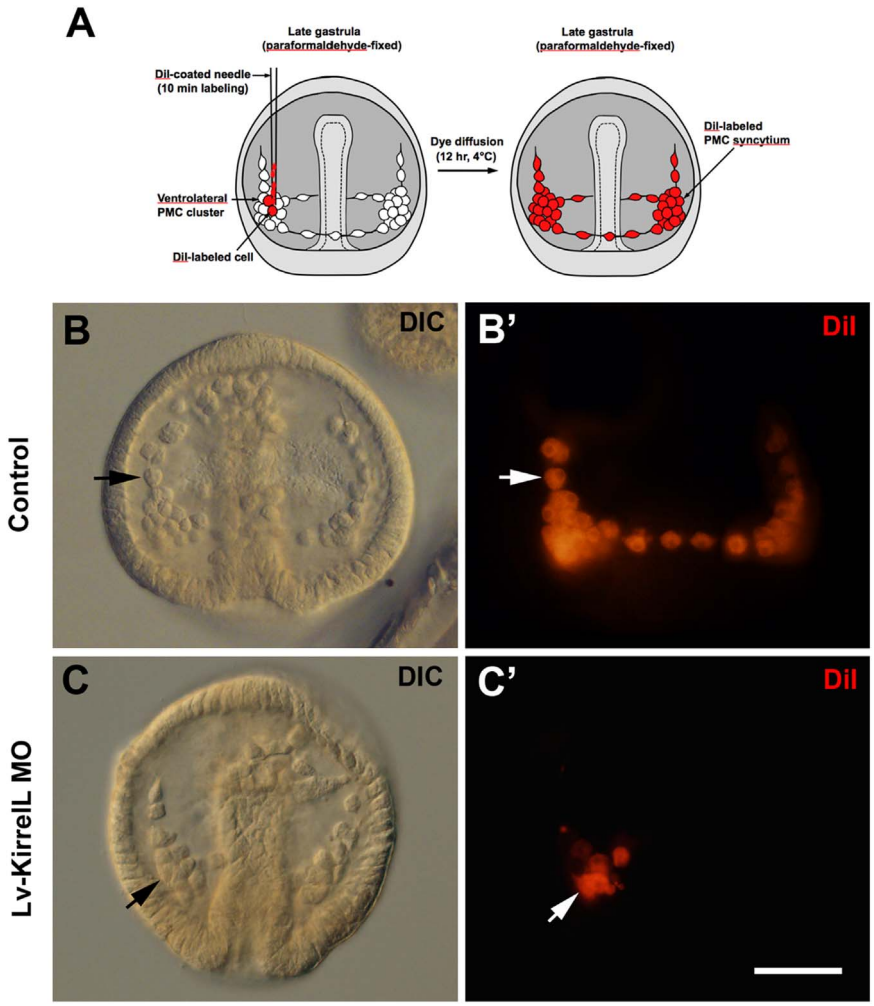

Fig. 5. PMCs do not form a syncytial network in Lv-KirrelL morphants. (A) Experimental procedure (Hodor and Ettensohn, 1998, 2008). Late gastrula stage *L. variegatus* embryos were fixed with 5% paraformaldehyde and a DiI-coated glass needle was pressed against several PMCs in one VLC for 10 min. After incubation overnight at 4 °C, embryos were examined by epifluorescence microscopy. (B, B′) Control embryo. DiI diffused from the VLC that was originally labeled (arrow) and spread throughout the PMC syncytium. (C, C′) Lv-KirrelL morphant embryo (2 mM). DiI remained restricted to a subset of PMCs within the VLC that was originally labeled (arrow). Scale bar=50 μm.

tions while GFP-tagged KirrelL transits the secretory pathway. At the resolution of the light microscope, our observations suggest that both cell surface and cortical pools of KirrelL protein are present. We did not detect ectopic cell fusion in embryos over-expressing KirrelL-GFP, probably because most cells in the embryo lack other molecules essential for cell fusion, such as direct membrane fusogens. When PMCs were isolated and cultured on fibronectin-coated coverslips, it was apparent that KirrelL-GFP decorated the entire cell body and was also distributed along the length of filopodia, consistent with a possible role in filopodial recognition (Fig. 8, C–D′).

3.5. IgTM is not required for PMC fusion but regulates the branching pattern of the skeletal primordia

During myoblast fusion, Ig-domain proteins mediate adhesion through heterophilic interactions with other members of this protein superfamily (Powell and Wright, 2011; Abmayr and Pavlath, 2012; Garrido-Urbani et al., 2014; Kim et al., 2015; Mandai et al., 2015). Recent high-throughput protein binding screens confirm that Ig-domain proteins often interact with other members of the superfamily (Özkan et al., 2013). We therefore explored the possibility that one of the three other PMC-specific, Ig-domain proteins might partner with KirrelL in mediating PMC fusion.

Injection of MOs targeted to *Lv-hypp_1164* and Lv-kirrel2L did not result in detectable effects on skeletogenesis or other aspects of embryo morphology. By contrast, Lv-IgTM morphants exhibited a striking skeletal phenotype, but one that differed from the phenotype of KirrelL morphants. During normal development, each spicule rudiment that forms within a VLC contains three branches separated by ~120° angles (Fig. 9, A, A′). IgTM knockdown led to the formation of spicule primordia with supernumerary branches, including tetraradiate, pentaradiate, and hexaradiate primordia (Fig. 9, B–D′). The frequency with which such primordia formed was dose-dependent and penetrance was somewhat variable among different batches of embryos, but across all experiments (3 trials, 2 mM MO) 30–70% of late gastrula-stage morphants exhibited at least one rudiment with supernumerary branches. The supernumerary branches were typically short and positioned between three longer arms that were separated by 120° angles. In addition, spicule branches were often wavy or curved in IgTM morphants, whereas in control embryos they were invariably straight. During later development, the supernumerary skeletal branches elongated to a limited extent but never reached lengths comparable to the three major branches (Fig. 9, E, E′). The morphogenesis of the remainder of the skeleton was normal and supernumerary skeletal rods were not observed in other regions. Immunostaining of Lv-IgTM morphants with mAb 6a9 showed that

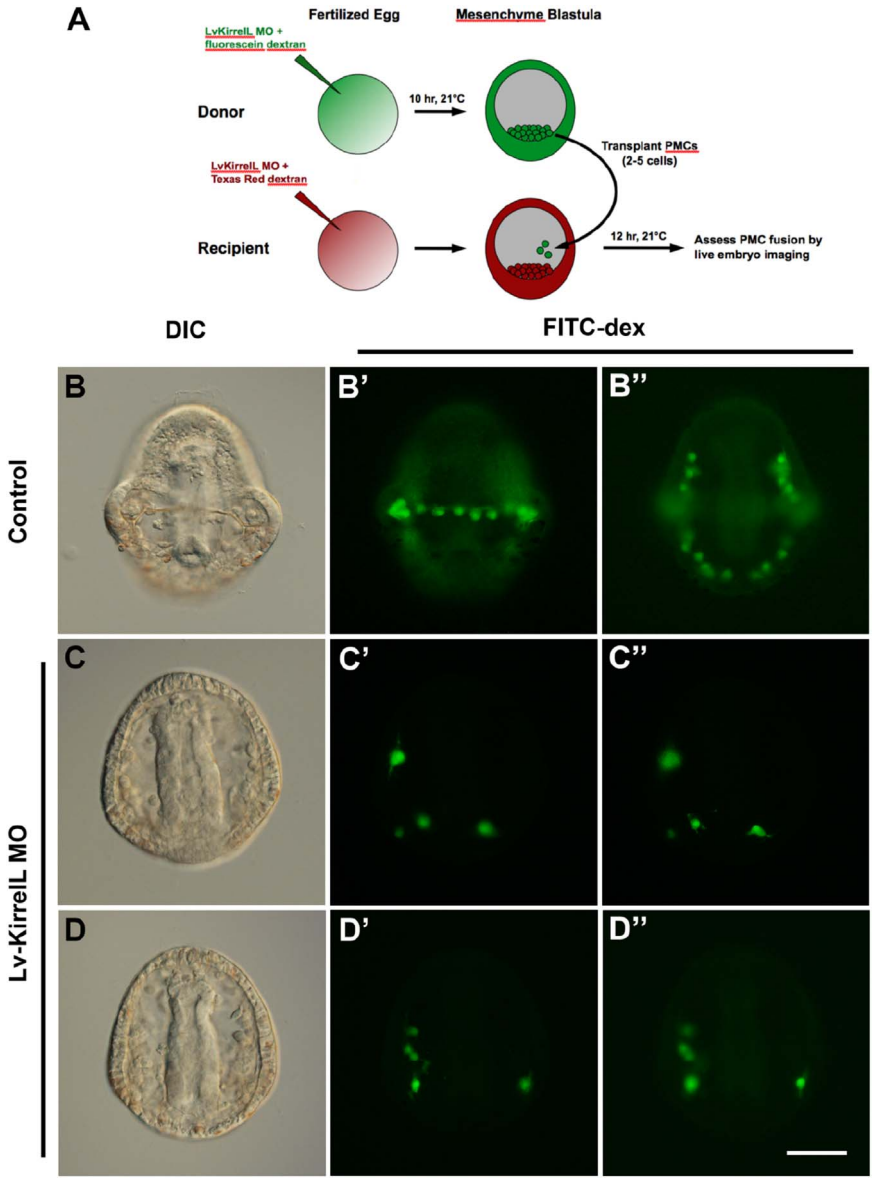

Fig. 6. Lv-KirrelL knockdown blocks PMC fusion. (A) Experimental procedure (after Hodor and Ettensohn (1998, 2008)). At the mesenchyme blastula stage, 2–5 fluorescein dextran-labeled PMCs were transplanted from a morphant embryo into a recipient (either a morphant or a control embryo) and PMC fusion was assessed by dye transfer. (B–B") Control (neither donor nor host injected with Lv-KirrelL MO). Fluorescent dextran was transferred from the donor cells to all PMCs as a result of cell fusion. (C–D") Two different morphant embryos. The original donor cells remained labeled, but dye was not transferred to other PMCs. Note after the 12 h incubation period, the labeled, donor PMCs were much brighter than those in control transplants due to the lack of dye diffusion, but exposure times were reduced in C′–D" to avoid blooming. Scale bar=50 μm.

the PMCs were organized in typical chains with well-formed pseudopodial cables, indicating that fusion was unaffected (Supp. Fig. 4A, B). We confirmed the IgTM knockdown phenotype in *S. purpuratus* embryos, using a MO that differed from the Lv-IgTM MO at 14/25 residues (Supp. Fig. 3C, C′).

Because MOs only partially block protein expression, we considered the possibility that, if KirrelL and IgTM interact, the distinctive IgTM morphant phenotype might result from incomplete inhibition of the interaction. The Lv-IgTM MO was tested at concentrations of 4 mM, 2 mM, 1 mM, and 500 μM; at the highest concentration, spicule rudiments with supernumerary branches formed, but the formation of the PMC syncytium was unaffected and many embryos also exhibited non-specific, toxic effects. This precluded the use of higher MO concentrations. An alternative approach was based on the reasoning that if IgTM and KirrelL are binding partners, and the IgTM morphant phenotype results from a partial inhibition of KirrelL-IgTM interactions, then an incomplete knockdown of Lv-KirrelL should phenocopy Lv-IgTM morphants. Titration of the Lv-KirrelL MO over a wide range of concentrations, however, (2 mM, 1 mM, 500 μM, 250 μM, and 125 μM) failed to induce supernumerary spicule branches at any concentration. At the lowest concentration tested (125 μM), all embryos formed normal tri-radiate spicule rudiments and skeletons. These findings show that IgTM plays a distinct role in regulating the initial branching pattern of the skeletal primordia but does not partner with KirrelL in mediating PMC fusion.

3.6. The evolution of PMC-specific Ig-domain proteins

A Clustal alignment of KirrelL proteins from *L. variegatus*, *S. purpuratus*, and *E. tribuloides* revealed a high degree of sequence conservation (Supp. Fig. 1). The divergence time between *L. variegatus* and *S. purpuratus* is approximately 100 MY (MY), while the divergence time between these species and *E. tribuloides* is >250 MY (Smith et al., 2006). All cysteine residues within the extracellular Ig domains

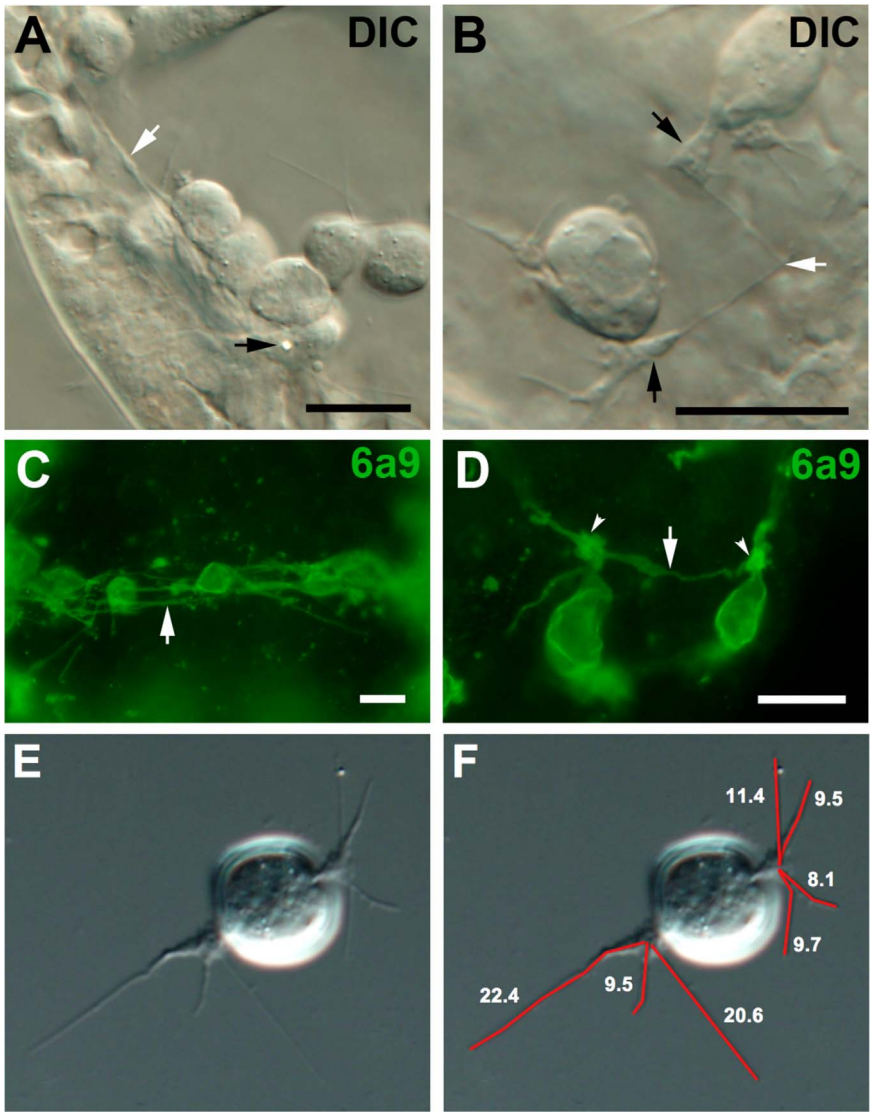

Fig. 7. Filopodial morphology and motility are unaffected by Lv-KirrelL knockdown. (A-D) Lv-KirrelL morphant embryos (2 mM), imaged when sibling controls were at the prism stage. (A, B) Living embryos, DIC optics. White arrows indicate filopodia and black arrows indicate broader cell protrusions (pseudopodia) from which filopodia typically extend, both in morphant and control embryos. In A, a small birefringent granule is visible within one such broad protrusion. In B, two filopodia extended by adjacent PMCs are in contact. (C, D) Fixed embryos immunostained with mAb 6a9. Arrows indicate filopodia and small arrowheads indicate pseudopodia. In C, a dense meshwork of filopodia is visible within the PMC band, but no pseudopodial cable has formed. In D, filopodia from two adjacent PMCs are in contact. (E, F) Quantification of PMC filopodial numbers and lengths *in vitro* (see Table 1). Shown is a PMC isolated from a KirrelL morphant embryo (*L. variegatus*) and cultured for 1 h on a fibronectin-coated coverslip. The lengths (in μm) of all filopodia extended by the cell, as measured using the ImageJ segmented line tool, are indicated in F. Scale bars=10 μm.

Table 1
Filopodial numbers and lengths in control PMCs and PMCs lacking KirrelL (*L. variegatus*).

	# Cells Scored	Total # Filopodia	# Filopodia/ Cell Mean (SD)	Filopodial Length Mean (SD)
Uninjected controls	100	419	4.2 (2.7)	11.4 μm* (6.6 μm)
KirrelL morphants	100	445	4.5 (2.6)	9.8 μm* (6.7 μm)

* Statistically significant difference ($p < 0.01$) by a two-sided *t*-test (equal variance).

were strictly conserved. Kocherlakota et al. (2008) carried out a mutational analysis of the cytoplasmic domain of Sticks-and-stones (Sns), an Ig-domain protein required for myoblast fusion in Drosophila, and showed that this region is phosphorylated at multiple tyrosine residues. Mutation of these sites compromised myoblast fusion, as did a double mutation of two consensus SH3 binding sites in the cytoplasmic domain. Putative phosphorylation sites in the cytoplasmic domain of Duf/Kirre are also required for this protein to mediate fusion (Bulchand et al., 2010). The cytoplasmic domains of the three sea urchin KirrelL proteins contained four strictly conserved tyrosine residues and many conserved serine and threonine residues, which are potential sites of phosphorylation. In addition, the cytoplasmic domains of the sea urchin proteins contained two conserved, consensus SH3 binding sites (PXXP). In Sns and nephrin, similar motifs are thought to bind to SH2/SH3 adaptor proteins that also interact with regulators of the actin cytoskeleton (Jones et al., 2006; Kaipa et al., 2013).

The sea urchin (*S. purpuratus*) genome encodes several hundred Ig domain-containing proteins, most of which also contain other domains commonly found in cell adhesion and extracellular proteins, such as EGF, FN3, and LRR domains (Whittaker et al., 2006). Domain annotation using SMART indicated that there are more than 50 Type

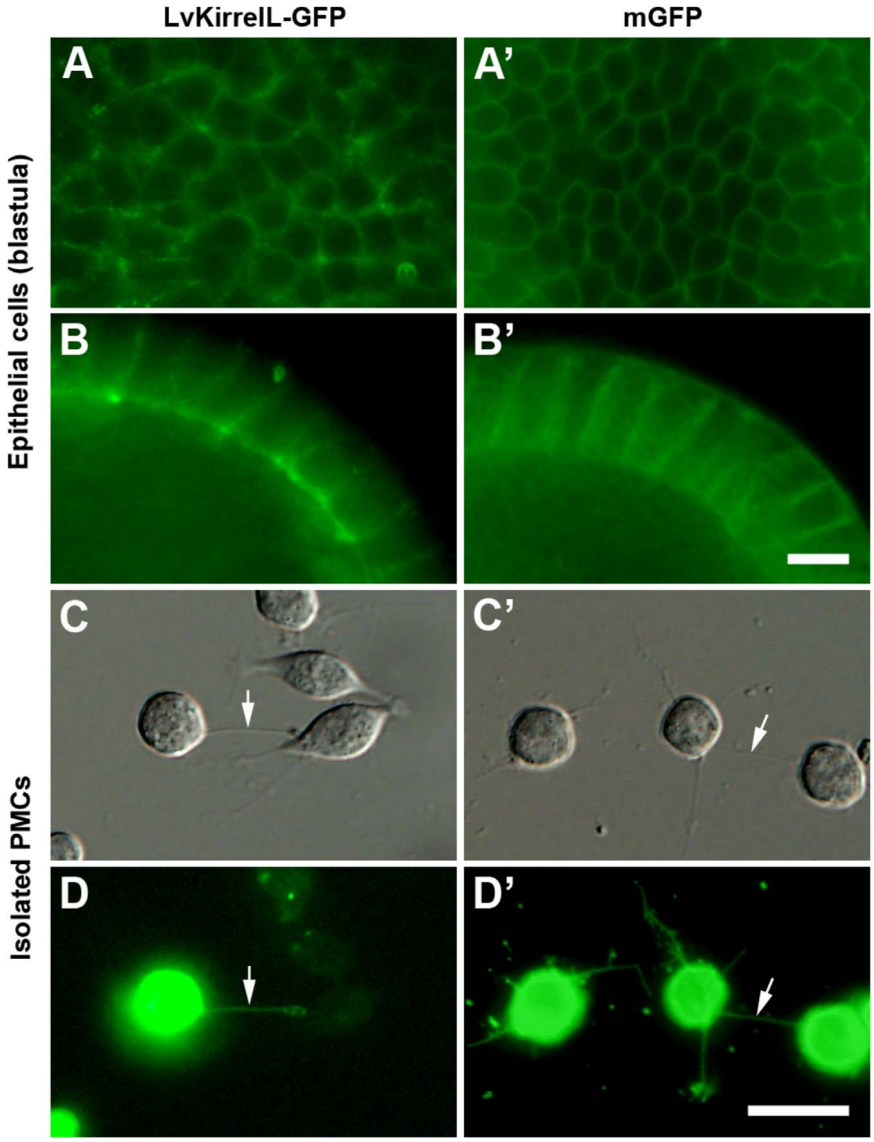

Fig. 8. Localization of LvKirrelL-GFP. The distributions of full-length, C-terminally GFP-tagged LvKirre (left column) and, for comparison, mGFP (right column) were examined in intact embryos (A–B′) and isolated PMCs cultured on fibronectin-coated coverslips (C–D′). In the epithelial cells of the blastula, LvKirrelL-GFP was concentrated at the cell periphery, predominantly in the basolateral region of the cells (B), but was less tightly restricted to the plasma membrane than mGFP (compare A and A′). In isolated PMCs, both proteins decorated filopodia (arrows) as well as cell bodies. Note that in D and D′ cell bodies appear highly flared due to the long exposure times required to reveal labeling of filopodia. Scale bars=10 μm.

I transmembrane proteins with extracellular regions that contain only Ig domains. BLAST-P analysis of the complete set of *S. purpuratus* proteins using full-length Sp-KirrelL as the query identified a subset of these proteins, all with 2–3 Ig domains, as the proteins most similar to Sp-KirrelL (E-values ranged from 10^{-20} to 10^{-40}) (Fig. 10; Supplemental File 1). Three of the corresponding genes (*Sp-hypp_880, Sp-hypp_1901*, and *Sp-hypp_2956*) are arranged in tandem on a single genomic scaffold, but the other genes are all located on different scaffolds. Unambiguous orthologs of most of these Ig-domain proteins were identified in other echinoids (*L. variegatus* and *E. tribuloides*) but, significantly, not in a non-echinoid echinoderm (*Patiria miniata*), two other invertebrate deuterostomes (*Saccoglossus kowalevskii* and *Branchiostoma floridae*) or vertebrates (Fig. 10). These findings point to an echinoid-specific diversification of the gene set (or an echinoderm-specific diversification, given that the annotation of the *Patiria* genome is incomplete and public genomic data for other echinoderms is limited). It was not possible to identify higher order relationships among the various echinoid-specific, Ig-domain proteins based on trees constructed using a variety of conditions, as bootstrap values were consistently very low (< 35). It was noteworthy that most of the genes that encode echinoid-specific Ig domain proteins lack introns, including all four genes expressed selectively by PMCs (Fig. 10). This was unexpected, as fewer than 9% of all *S. purpuratus* genes lack introns (Zou et al., 2011). Lack of introns is a hallmark of genes that have arisen via retrotransposition, a common mechanism of gene birth, and sea urchin genes encoding Ig domain proteins may have diversified by this mechanism (Babushok et al., 2007; Chen et al., 2011; Long et al., 2013).

4. Discussion

4.1. Ig domain proteins and cell fusion

Ig domain-containing proteins constitute one of the major families of cell adhesion molecules (Ig-CAMs) and play important roles in the morphogenesis of diverse tissues (Kamiguchi and Lemmon, 2000;

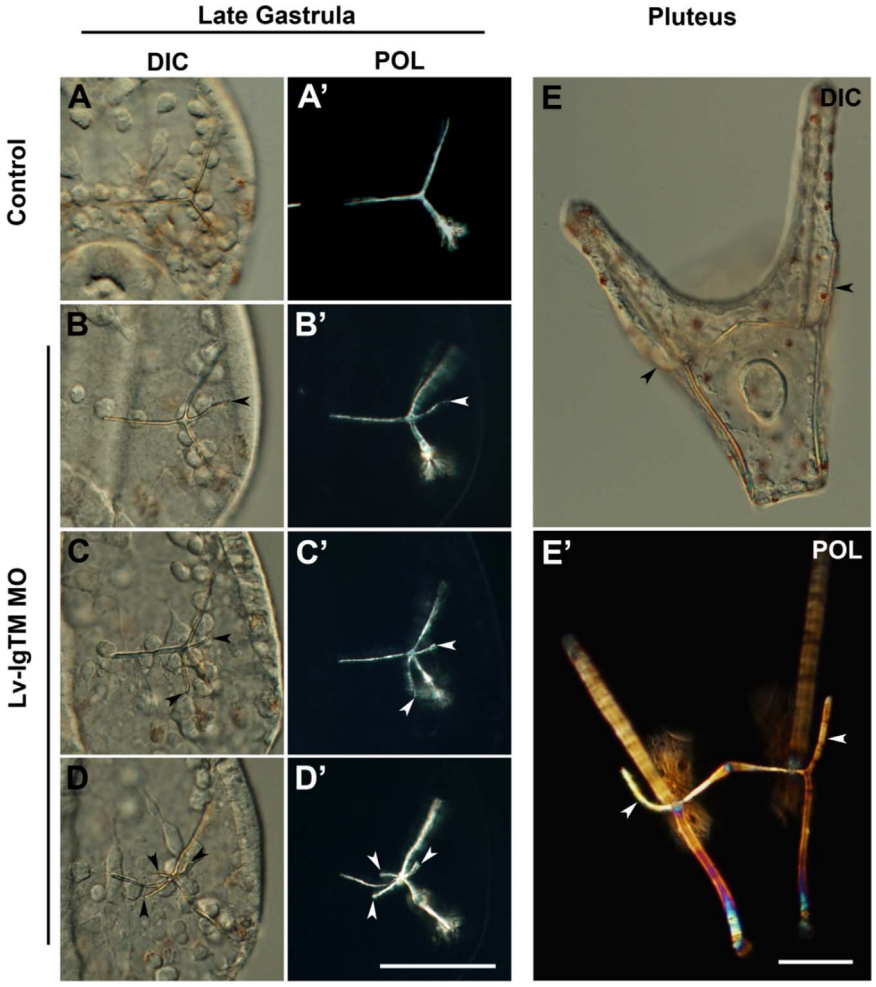

Fig. 9. IgTM regulates regulates the branching pattern of the two skeletal primodia. *L. variegatus* embryos were viewed with DIC and polarization optics (paired images of the same embryos). In late gastrula stage controls (A, A′), each spicule rudiment formed three branches at ~120° angles. IgTM knockdown led to the formation of tetraradiate (B, B′), pentaradiate (C, C′) and hexaradiate (D, D′) spicule primordia. Supernumerary branches (arrowheads) were usually short and appeared to lie between three longer arms. The supernumerary branches elongated but not to the extent of the three major arms, and the subsequent branching of the skeleton was normal (E, E′). Scale bars=50 μm.

Bazzoni, 2003; Volkmer et al., 2013; Ristola and Lehtonen, 2014). The role of Ig-domain proteins has been studied intensively in the context of myogenesis, one of the best understood experimental models of cell-cell fusion (Abmayr and Pavlath, 2012; Kim et al., 2015). Genetic and molecular studies of myoblast fusion have revealed a multi-step process involving 1) cell recognition and adhesion, 2) enhancement of plasma membrane apposition, and 3) destabilization and fusion of lipid bilayers. In both vertebrates and invertebrates, immunoglobulin (Ig) domain-containing transmembrane proteins play an essential role during the initial (cell recognition) phase of myoblast fusion. Knockout studies have shown that Ig-domain proteins are required for myoblast fusion in Drosophila and vertebrates (Srinivas et al., 2007; Sohn et al., 2009; Powell and Wright, 2011; Abmayr and Pavlath, 2012) and forced expression of Ig-domain proteins is sufficient to induce cell fusion in some non-fusogenic cell lines (Shilagardi et al., 2013; Zhuang et al., 2015). During myoblast fusion, Ig domain-containing proteins probably facilitate close cell-cell contacts that allow other membrane proteins to trigger bilayer fusion (Özkan et al., 2014; Podbilewicz, 2014; Kim et al., 2015). The role of Ig domain proteins in the fusion of non-muscle lineages is unknown, although one study has suggested that SnS may also contribute to the formation of binucleate nephrocytes (Zhuang et al., 2009). Our findings demonstrate clearly that KirrelL is essential for cell-cell fusion in a non-muscle embryonic lineage and point to a widely conserved role for Ig domain proteins in cell fusion.

4.2. PMC fusion and the role of KirrelL

Sea urchin skeletogenic cells are organized as syncytia not only in the embryo but also in biomineralizing tissues of adults (Kniprath, 1974; Märkel et al., 1986). It has been speculated that cell fusion is required for skeletogenesis by facilitating the formation of an expansive, partially membrane-bound compartment within which skeletal elements can be deposited (Wilt and Ettensohn, 2007). Our finding that only small biomineral elements form when PMC fusion is blocked provides the first direct experimental support for this view. Moreover, in morphant embryos that exhibit an intermediate phenotype and form relatively short, linear skeletal rods, such rods are invariably associated with small PMC syncytia consisting of several cells.

Okazaki (1965) made continuous, transmitted light observations of PMC behavior and found that the formation of the PMC syncytium is a multistep process. She observed contacts between the tips of filopodia followed by filopodial shortening and the eventual coalescence of broader cell protrusions (pseudopodia) from which the filopodia project. This distinctive fusion behavior produces the pseudopodial cables that join PMCs to one another. From brightfield imaging alone it is not possible to determine when membrane fusion occurs, but continuous observations of PMCs labeled with fluorescent dextran suggest that, at least in some cases, PMC membranes fuse during the initial phase of filopodial contact, prior to the amalgamation of the pseudopodia (Hodor and Ettensohn, 1998).

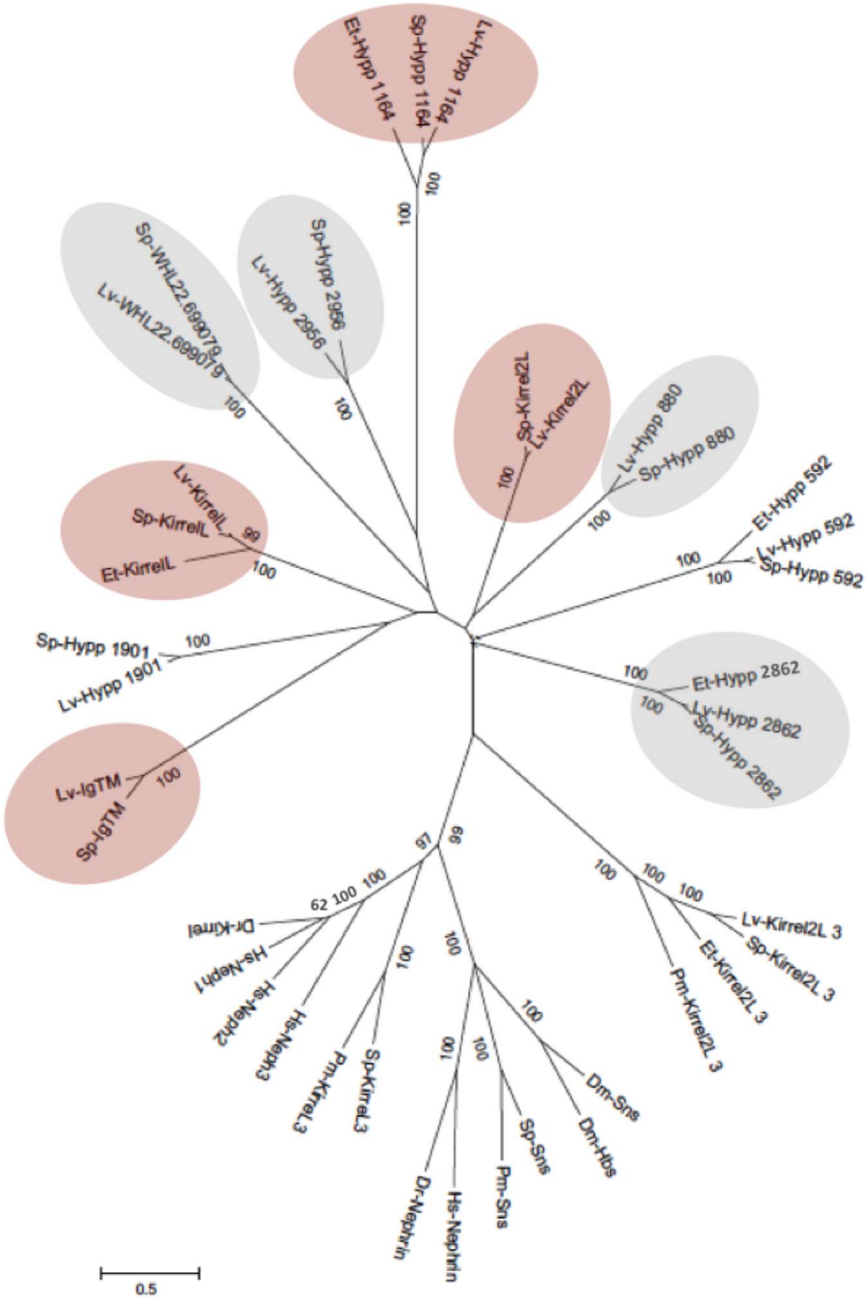

Fig. 10. Unrooted, maximum likelihood tree showing the four PMC-specific Ig-domain proteins (shaded in red) and closely related sea urchin proteins. All proteins shown are predicted to be Type I transmembrane proteins with a signal sequence, two or more extracellular Ig domains, a transmembrane domain, and a cytoplasmic domain. Genes in shaded ovals (red or gray) lack introns. Only bootstrap value greater than 35 are shown. The tree also includes sea urchin orthologs of Ig domain-containing proteins that mediate myoblast fusion (Sns/Nephrin in Drosophila and vertebrates, and Kirrel in zebrafish). Dm- *Drosophila melanogaster*, Dr- *Danio rerio*, Et- *Eucidaris tribuloides,* Hs – *Homo sapiens, Lv – Lytechinus variegatus, Pm – Patiria minata, Sp – Strongylocentrotus purpuratus*. All protein sequences used for tree construction are shown in Supplemental File 1.

Our observations of living and 6a9-stained embryos indicate that PMC specification, division, ingression, and directional migration to the subequatorial region of the blastocoel wall all occur normally in Lv-KirrelL morphants. In addition, PMC filopodia extend and contact one another, although cell fusion does not occur. The predicted structure of the KirrelL protein and the targeting of a GFP-tagged form of the protein to the PMC surface, including filopodial cell protrusions, support the hypothesis that KirrelL functions as a cell recognition or adhesion molecule. We therefore hypothesize that PMC-PMC adhesion mediated by KirrelL is required for filopodia contacts to result in membrane fusion. It seems likely that, as in other experimental models, other proteins (membrane fusogens) mediate the final step in the fusion process; i.e., the merging of the lipid bilayers of the two cells. It is noteworthy that recent studies have called attention to the role of actin-rich protrusions in facilitating myoblast fusion, possibly by promoting the engagement of fusogenic membrane proteins (Shilagardi et al., 2013; Haralalka et al., 2014).

Ig domain proteins engage both in homophilic binding interactions and in heterophilic interactions with other Ig domain proteins (Özkan et al., 2013). Our experiments suggest that none of the other known PMC-specific Ig-domain proteins functions as an essential binding partner for KirrelL. Moreover, we find that expression of KirrelL on one fusion partner is not sufficient to induce fusion; the protein must be expressed by both cells. These findings are most easily explained by a homophilic binding mechanism but do not rigorously exclude other possible models.

Late in gastrulation, other migratory mesenchyme cells (blastocoelar cells, or BCs) fuse with one another, producing large, multinucleate cells (Hodor and Ettensohn, 1998). PMCs and BCs come into direct contact with one another when both cell types are fusogenic, yet such filopodial contacts never result in PMC-BC fusion. The findings reported here can account for the strict cell-type specificity of cell fusion if KirrelL, a PMC-specific protein, interacts in a homophilic manner or with a binding partner not expressed by BCs. Several other proteins with domain structures very similar to KirrelL are expressed during gastrulation; one or more of these proteins may be restricted to BCs and mediate the fusion of these cells.

4.3. IgTM and the branching pattern of the spicule rudiment

The phenotype of IgTM morphants demonstrates that this protein ordinarily functions to limit the number of branches in the spicule rudiment to three. Little is known concerning the mechanisms that regulate the initial branching pattern of the rudiment. Isolated micromeres produce tri-radiate spicules in culture, demonstrating that no spatially organized patterning information from other tissues is required (Okazaki, 1975). High concentrations of serum or vascular endothelial growth factor (VEGF), which is likely to be one of the active factors in serum, favor the formation of tri-radiate spicules in culture rather than linear spicules (Kinoshita and Okazaki, 1984; Knapp et al., 2012). These two morphological forms grow parallel to the c- and a-crystallographic axes, respectively, and therefore the effect of VEGF/serum appears to be to regulate the axial orientation of crystal growth. No conditions other than IgTM knockdown, however, have been shown to alter the number of branches of spicule rudiments that extend along the a-axis.

4.4. Linking the PMC GRN to morphogenesis

Although the transcriptional network that underlies PMC specification has recently been linked to many biomineralization-related genes (Rafiq et al., 2012, 2014), identifying effector genes in the network that control other aspects of PMC morphogenesis has proven more challenging. One effector of known morphogenetic function is *vegfr-Ig-10*, which encodes a receptor tyrosine kinase that mediates PMC guidance (Duloquin et al., 2007; Adomako-Ankomah et al., 2013). In the present study, we have identified a second effector, KirrelL, that regulates an essential morphogenetic behavior of PMCs. *kirrelL* is downstream of both Alx1 and Ets1 in the PMC GRN, as shown by a dramatic (> 95%) reduction in the level of *kirrelL* mRNA following knockdown of either transcription factor (Rafiq et al., 2014). The identification of additional morphogenetic effector genes (including genes that participate with KirrelL in mediating PMC fusion) and an elucidation of their regulatory control will further expand our view of the genetic control of anatomy in this experimental model.

Acknowledgements

We thank Dr. D. Durand for advice concerning protein evolution and phylogenetic tree construction, D. R. McClay for providing the mGFP plasmid, and R. A. Cameron for identifying the full-length coding sequence of KirrelL from *Eucidaris tribuloides*.

This work was supported by Grant IOS-1354973 from the National Science Foundation, United States.

Appendix A. Supporting information

Supplementary data associated with this article can be found in the online version at doi:10.1016/j.ydbio.2016.11.006.

References

Abmayr, S.M., Pavlath, G.K., 2012. Myoblast fusion: lessons from flies and mice. Development 139, 641–656.
Adomako-Ankomah, A., Ettensohn, C.A., 2013. Growth factor-mediated mesodermal cell guidance and skeletogenesis during sea urchin gastrulation. Development 140 (20), 4214–4225.
Babushok, D.V., Ostertag, E.M., Kazazian, H.H., Jr., 2007. Current topics in genome evolution: molecular mechanisms of new gene formation. Cell Mol. Life Sci. 64, 542–554.
Barsi, J.C., Tu, Q., Davidson, E.H., 2014. General approach for in vivo recovery of cell type-specific effector gene sets. Genome Res. 24, 860–868.
Bazzoni, G., 2003. The JAM family of junctional adhesion molecules. Curr Opin Cell Biol. 15 (5), 525–530.
Bulchand, S., Menon, S.D., George, S.E., Chia, W., 2010. The intracellular domain of Dumbfounded affects myoblast fusion efficiency and interacts with Rolling pebbles and Loner. PLoS One 20105 (2), e9374.
Cameron, R.A., Samanta, M., Yuan, A., He, D., Davidson, E.H., 2009. SpBase: the sea urchin genome database and web site. Nucleic Acids Res. 37, D750–D754.
Cheers, M.S., Ettensohn, C.A., 2004. Rapid microinjection of fertilized eggs. Methods Cell Biol. 74, 287–310.
Chen, M., Zou, M., Fu, B., Li, X., Vibranovski, M.D., Gan, X., Wang, D., Wang, W., Long, M., He, S., 2011. Evolutionary patterns of RNA-based duplication in non-mammalian chordates. PLoS One 6, e21466.
De Bruyn, A., Martin, D.P., Lefeuvre, P., 2014. Phylogenetic reconstruction methods: an overview. Methods Mol. Biol. 1115, 257–277.
Duloquin, L., Lhomond, G., Gache, C., 2007. Localized VEGF signaling from ectoderm to mesenchyme cells controls morphogenesis of the sea urchin embryo skeleton. Development 134, 2293–2302.
Erkenbrack, E.M., Davidson, E.H, 2015. Evolutionary rewiring of gene regulatory network linkages at divergence of the echinoid subclasses. Proc. Natl. Acad. Sci. USA 112, E4075-84.
Ettensohn, C.A., 2013. Encoding anatomy: developmental gene regulatory networks and morphogenesis. Genesis 51, 383–409.
Ettensohn, C.A., 2014. Horizontal transfer of the msp130 gene supported the evolution of metazoan biomineralization. Evol Dev. 16, 139–148.
Garrido-Urbani, S., Bradfield, P.F., Imhof, B.A., 2014. Tight junction dynamics: the role of junctional adhesion molecules (JAMs). Cell Tissue Res. 355, 701–715.
Gibbins, J.R., Tilney, L.G., Porter, K.R., 1969. Microtubules in the formation and development of the primary mesenchyme in *Arbacia punctulata*. I. The distribution of microtubules. J. Cell Biol. 41, 201–226.
Gustafson, T., Wolpert, L., 1961. Studies on the cellular basis of morphogenesis in the sea urchin embryo. Directed movements of primary mesenchvme cells in normal and vegetalized larvae. Exp. Cell Res 24, 64–79.
Hall, B.G., 2013. Building phylogenetic trees from molecular data with MEGA. Mol Biol Evol. 30, 1229–1235.
Haralalka, S., Shelton, C., Cartwright, H.N., Guo, F., Trimble, R., Kumar, R.P., Abmayr, S.M., 2014. Live imaging provides new insights on dynamic F-actin filopodia and differential endocytosis during myoblast fusion in Drosophila. PLoS One 9, e114126.
Hodor, P.G., Ettensohn, C.A., 1998. The dynamics and regulation of mesenchymal cell fusion in the sea urchin embryo. Dev. Biol. 199, 111–124.
Hodor, P.G., Ettensohn, C.A., 2008. Mesenchymal cell fusion in the sea urchin embryo. Methods Mol. Biol. 475, 315–334.
Jones, N., Blasutig, I.M., Eremina, V., Ruston, J.M., Bladt, F., Li, H., Huang, H., Larose, L., Li, S.S., Takano, T., Quaggin, S.E., Pawson, T., 2006. Nck adaptor proteins link nephrin to the actin cytoskeleton of kidney podocytes. Nature 440, 818–823.
Kaipa, B.R., Shao, H., Schäfer, G., Trinkewitz, T., Groth, V., Liu, J., Beck, L., Bogdan, S., Abmayr, S.M., Önel, S.F., 2013. Dock mediates Scar- and WASp-dependent actin polymerization through interaction with cell adhesion molecules in founder cells and fusion-competent myoblasts. J. Cell Sci. 126, 360–372.
Kamiguchi, H., Lemmon, V., 2000. IgCAMs: bidirectional signals underlying neurite growth. Curr. Opin. Cell Biol. 12, 598–605.
Karp, G.C., Solursh, M., 1985a. In vitro fusion and separation of sea urchin primary mesenchyme cells. Exp. Cell Res. 158, 554–557.
Karp, G.C., Solursh, M., 1985b. Dynamic activity of the filopodia of sea urchin embryonic cells and their role in directed migration of the primary mesenchyme *in vitro*. Dev. Biol. 112, 276–283.
Kim, J.H., Jin, P., Duan, R., Chen, E.H., 2015. Mechanisms of myoblast fusion during muscle development. Curr. Opin. Genet. Dev. 32, 162–170.
Kinoshita, T., Okazaki, K., 1984. *In vitro* study on morphogenesis of sea urchin larval spicule: adhesiveness of cells. Zool. Sci. 1, 433–443.
Knapp, R.T., Wu, C.H., Mobilia, K.C., Joester, D., 2012. Recombinant sea urchin vascular endothelial growth factor directs single-crystal growth and branching in vitro. J. Am. Chem. Soc. 134, 17908–17911.
Kniprath, E., 1974. Ultrastructure and growth of the sea urchin tooth. Calcif. Tissue Res 14, 211–228.
Kocherlakota, K.S., Wu, J.M., McDermott, J., Abmayr, S.M., 2008. Analysis of the cell adhesion molecule sticks-and-stones reveals multiple redundant functional domains, protein-interaction motifs and phosphorylated tyrosines that direct myoblast fusion in Drosophila melanogaster. Genetics 178, 1371–1383.
Koga, H., Fujitani, H., Morino, Y., Miyamoto, N., Tsuchimoto, J., Shibata, T.F., Nozawa, M., Shigenobu, S., Ogura, A., Tachibana, K., Kiyomoto, M., Amemiya, S., Wada, H., 2016. Experimental approach reveals the role of *alx1* in the evolution of the echinoderm larval skeleton. PLoS One 11, e0149067.

Long, M., VanKuren, N.W., Chen, S., Vibranovski, M.D., 2013. New gene evolution: little did we know. Annu. Rev. Genet. 47, 307–333.
Lyons, D.C., Martik, M.L., Saunders, L.R., McClay, D.R., 2014. Specification to biomineralization: following a single cell type as it constructs a skeleton. Integr. Comp. Biol. 54, 723–733.
Mandai, K., Rikitake, Y., Mori, M., Takai, Y., 2015. Nectins and nectin-like molecules in development and disease. Curr. Top. Dev. Biol. 112, 197–231.
Märkel, K., Roeser, U., Mackenstedt, U., Klostermann, M., 1986. Ultrastructural investigation of matrix-mediated biomineralization in echinoids (Echinodermata, Echinoidea). Zoomorph 106, 232–243.
Okazaki, K., 1965. Skeleton formation of sea urchin larvae. V. Continuous observation of the process of matrix formation. Exp. Cell Res. 40, 585–596.
Okazaki, K., 1975. Spicule formation by isolated micromeres of the sea urchin embryo. Am. Zool. 15, 567–581.
Oliveri, P., Tu, Q., Davidson, E.H., 2008. Global regulatory logic for specification of an embryonic cell lineage. Proc. Natl. Acad. Sci. USA 105, 5955–5962.
Özkan, E., Carrillo, R.A., Eastman, C.L., Weiszmann, R., Waghray, D., Johnson, K.G., Zinn, K., Celniker, S.E., Garcia, K.C., 2013. An extracellular interactome of immunoglobulin and LRR proteins reveals receptor-ligand networks. Cell 154, 228–239.
Özkan, E., Chia, P.H., Wang, R.R., Goriatcheva, N., Borek, D., Otwinowski, Z., Walz, T., Shen, K., Garcia, K.C., 2014. Extracellular architecture of the SYG-1/SYG-2 adhesion complex instructs synaptogenesis. Cell 156, 482–494.
Penn, O., Privman, E., Ashkenazy, H., Landan, G., Graur, D., Pupko, T., 2010. GUIDANCE: a web server for assessing alignment confidence scores. 2010 38(Web Server issue):W23-8.. Nucleic Acids Res. 38 (Web Server issue), w23–w28.
Podbilewicz, B., 2014. Virus and cell fusion mechanisms. Annu. Rev. Cell Dev. Biol. 30, 111–139.
Powell, G.T., Wright, G.J., 2011. Jamb and jamc are essential for vertebrate myocyte fusion. PLoS Biol. 9, e1001216.
Rafiq, K., Cheers, M., Ettensohn, C.A., 2012. The genomic regulatory control of skeletal morphogenesis in the sea urchin. Development 139, 579–590.
Rafiq, K., Shashikant, T., McManus, C.J., Ettensohn, C.A., 2014. Genome-wide analysis of the skeletogenic gene regulatory network of sea urchins. Development 141, 950–961.
Ristola, M., Lehtonen, S., 2014. Functions of the podocyte proteins nephrin and Neph3 and the transcriptional regulation of their genes. Clin. Sci. 126, 315–328.
Saunders, L.R., McClay, D.R., 2014. Sub-circuits of a gene regulatory network control a developmental epithelial-mesenchymal transition. Development 141, 1503–1513.
Shilagardi, K., Li, S., Luo, F., Marikar, F., Duan, R., Jin, P., Kim, J.H., Murnen, K., Chen, E.H., 2013. Actin-propelled invasive membrane protrusions promote fusogenic protein engagement during cell-cell fusion. Science 340, 359–363.
Sievers, F., Wilm, A., Dineen, D., Gibson, T.J., Karplus, K., Li, W., Lopez, R., McWilliam, H., Remmert, M., Söding, J., Thompson, J.D., Higgins, D.G., 2011. Fast, scalable generation of high-quality protein multiple sequence alignments using Clustal Omega. Mol. Syst. Biol. 7, 539.
Smith, A.B., Pisani, D., Mackenzie-Dodds, J.A., Stockley, B., Webster, B.L., Littlewood, D.T., 2006. Testing the molecular clock: molecular and paleontological estimates of divergence times in the Echinoidea (Echinodermata). Mol. Biol. Evol. 23, 1832–1851.
Sohn, R.L., Huang, P., Kawahara, G., Mitchell, M., Guyon, J., Kalluri, R., Kunkel, L.M., Gussoni, E., 2009. A role for nephrin, a renal protein, in vertebrate skeletal muscle cell fusion. Proc. Natl. Acad. Sci. USA 106, 9274–9279.
Srinivas, B.P., Woo, J., Leong, W.Y., Roy, S.A., 2007. A conserved molecular pathway mediates myoblast fusion in insects and vertebrates. Nat. Genet. 39, 781–786.
Summerton, J., 1999. Morpholino antisense oligomers: the case for an RNase H-independent structural type. Biochim. Biophys. Acta 1489, 141–158.
Tamura, K., Peterson, D., Peterson, N., Stecher, G., Nei, M., Kumar, S., 2011. MEGA5: molecular evolutionary genetics analysis using maximum likelihood, evolutionary distance, and maximum parsimony methods. Mol Biol Evol. 28, 2731–2739.
Théel, H., 1892. On the development of Echinocyamus pusillus. Nova Acta R. Soc. Sci. Upsal. Ser. III, 1–57.
Tu, Q., Cameron, R.A., Davidson, E.H., 2014. Quantitative developmental transcriptomes of the sea urchin *Strongylocentrotus purpuratus*. Dev. Biol. 385, 160–167.
Volkmer, H., Schreiber, J., Rathjen, F.G., 2013. Regulation of adhesion by flexible ectodomains of IgCAMs. Neurochem. Res. 38, 1092–1099.
Whittaker, C.A., Bergeron, K.F., Whittle, J., Brandhorst, B.P., Burke, R.D., Hynes, R.O., 2006. The echinoderm adhesome. Dev. Biol. 300, 252–266.
Wilt, F.H., Ettensohn, C.A., 2007. The morphogenesis and biomineralization of the sea urchin larval skeleton. In: Bauerlein, E. (Ed.), Handbook of Biomineralization: Biological Aspects and Structure Formation. Wiley-VCH Press, Weinheim, Germany, 183–210.
Zhuang, L., Pandey, A.V., Villiger, P.M., Trueb, B., 2015. Cell-cell fusion induced by the Ig3 domain of receptor FGFRL1 in CHO cells. Biochim. Biophys. Acta 1853, 2273–2285.
Zhuang, S., Shao, H., Guo, F., Trimble, R., Pearce, E., Abmayr, S.M., 2009. Sns and Kirre, the Drosophila orthologs of Nephrin and Neph1, direct adhesion, fusion and formation of a slit diaphragm-like structure in insect nephrocytes. Development 136, 2335–2344.
Zou, M., Guo, B., He, S., 2011. The roles and evolutionary patterns of intronless genes in deuterostomes. Comp. Funct. Genom. 2011, 680673.